INTERNATIONAL JOURNAL FOR NUMERICAL METHODS IN FLUIDS
Int. J. Numer. Meth. Fluids 2015; **77**:707–731
Published online 11 February 2015 in Wiley Online Library (wileyonlinelibrary.com). DOI: 10.1002/fld.4000

A simple hybrid finite volume solver for compressible turbulence

V. Kalyana Chakravarthy*,†, K. Arora and D. Chakraborty

Defence Research Development Laboratory, Kanchanbagh, Hyderabad 500058, India

SUMMARY

A simple, explicit, hybrid finite volume method for simulating compressible turbulence is developed by combining a fourth-order central scheme and a shock-capturing simple low-dissipation advection upstream splitting method. The total flux on each of the cell faces is computed as a weighted average of central/nondissipative and upwind/dissipative fluxes. The weights are determined using an unphysical oscillation sensor in addition to a more traditional discontinuity sensor used in earlier studies. Shocks are well captured, but overshoots in density are predicted around contact discontinuities that are normal to the flow. The use of the latter sensor effectively prevents these overshoots from generating spurious oscillations that travel away from the contact lines. The efficacy of the proposed method for direct or large-eddy simulations of supersonic turbulence is established using several canonical test problems. Copyright © 2015 John Wiley & Sons, Ltd.

Received 16 July 2014; Revised 26 October 2014; Accepted 13 December 2014

KEY WORDS: shock capturing; turbulence; numerical oscillations

1. INTRODUCTION

Direct numerical simulation (DNS) and large eddy simulation (LES) have increased the predictability of turbulent flows significantly over what is possible with Reynolds averaged approaches. Much of the work on these approaches has focused on incompressible flows. For such flows, keeping the dissipation associated with numerics of non-viscous (and in case of LES, non-subgrid) terms minimal is a key requirement. This can be met by using very-high-order upwind-biased schemes that are slightly dissipative or dispersive central schemes for discretizing the advection terms. The central schemes were shown to be better especially if the small-scale dynamics are important like in reacting flows [1]. In fact, schemes that conserve kinetic energy exactly in the inviscid limit have been developed [2] and extended later for compressible flows [3, 4]. Compact schemes [5] that provide good resolution over a broad range of scales are alternatives to these schemes, although more recent upwind versions have some slight amount of dissipation. These schemes or any nondissipative ones cannot be used for supersonic flows because they generate numerical oscillations around shocks and contact lines. Numerical dissipation is needed to capture these discontinuities. The numerical dissipation should be highly localized around discontinuities. Otherwise, it would damp out physical oscillations needed to model the turbulent energy cascade.

For capturing shocks in turbulence simulations, four approaches are commonly used [6]. The artificial dissipation approaches based on work by Jameson and coworkers in the context of Euler and Reynolds averaged Navier–Stokes solvers have now been tailored for use in LES [7–11]. In the context of LES, they are referred to as hyperviscosity approaches. Several hyperviscosity expressions have been proposed which act selectively in the vicinity of shocks to keep the numerical

*Correspondence to: V. K. Chakravarthy, Defence Research Development Laboratory, Kanchanbagh, Hyderabad 500058, India.
†E-mail: v_kalyana_chakravarthy@yahoo.co.in

oscillations generated by the baseline nondissipative scheme under check while retaining the physical turbulent fluctuations intact. Fu and Ma [12] identified nonuniform group velocity distribution as the origin of these numerical oscillations and proposed appropriately designed hyperviscosity expressions as a way of controlling it. Their expressions turned out to be a bit more complex than the ones based on the work of Cook and coworkers, which are most commonly used [7–11]. The hyperviscosity terms usually have adjustable constants that are not universal; that is, the adjustable constants may depend on the stencils used for computing hyperdiffusion terms [10]. These approaches have mostly been implemented using compact schemes. When using a noncompact baseline scheme, the form of hyperdiffusion terms or at least the numerical constants in them may need to be modified. Sometimes, an additional filtering step to remove poorly resolved oscillations away from shocks is also needed [13, 14]. It is to be noted that parallelization of compact schemes on distributed memory architecture-based machines is not as straightforward as it is for fully explicit methods.

Flux split schemes whose construction relies on the hyperbolic characteristic nature of Euler equations are commonly used for capturing shocks effectively. Higher-order extensions to flux split schemes are achieved mostly using the Monotonic Upstream-centered Scheme for Conservation Laws (MUSCL), essentially nonoscillatory (ENO) or weighted ENO (WENO) approaches. The MUSCL approach is relatively simple and generally limited to spatially second order at most. Order of accuracy as high as seven has been reported for some of the ENO/WENO approaches. Being only second order accurate, MUSCL-based flux split schemes by themselves are too dissipative and unsuitable for turbulence computations. WENO schemes are significantly more complex and are still being refined with choice of interpolation stencils, smoothness indicators being the areas of focus [15, 16]. WENO schemes have been proposed for use in LES because of their higher-order nature in smooth regions, but some have argued [6, 11, 17] that they are still too dissipative for LES in regions away from shocks. They are mostly used in the context of LES as parts of hybrid solvers. A nondissipative scheme, typically compact, is hybridized with a ENO/WENO scheme to arrive at a high-resolution LES solver [17–19]. Such solvers are very complex, hard to develop and still not fully without problems. For example, the nonoscillatory nature of ENO/WENO schemes is generally based on one-dimensional constructions along grid lines. In multidimensional simulations, however, oscillations can appear [15] because the multidimensional extensions may not necessarily be nonoscillatory. With additional complexity, quadrature terms can be added to render multidimensional nonoscillatory nature. Some of the kinetic energy-preserving schemes have also been hybridized with flux split schemes [20, 21]. The main challenge for hybrid schemes is detection of shocks and localization of numerical dissipation around them.

Another approach for high-speed LES is based on explicit filtering pioneered by Adam, Stolz, and their coworkers [22–25], which seeks to filter solutions obtained using higher-order central schemes to get rid of oscillations they generate around shocks. An integrated approach where such filtering, in addition, would account for the effect of unresolved subgrid scales was also developed and used to perform LES of several supersonic flows. This is facilitated by the fact that lack of sufficient resolution to resolve dissipation range of scales results in high-wavenumber oscillations similar to ones created when using nondissipative schemes to capture shocks. However, two filters are needed in this approach, and local adaptation of the secondary filter was found to be necessary for capturing shock turbulence interactions accurately [24]. Integrated modeling of shocks and subgrid effects is not unique to filtering approaches. It is also performed using hyperdiffusivity approaches described earlier, but this has been questioned recently in the context of high Reynolds flows [26], and the methodology continues to be refined [27, 28].

Recent approaches based on characteristic filtering [14, 29, 30], which do not depend on WENO schemes, seem very promising for LES and are becoming increasingly popular. They, however, still rely on compact schemes for baseline solvers. Numerical oscillations that are generated far from shocks have to be controlled by biasing the compact scheme [29, 30] or by using an additional low-pass filtering step [14].

It is clear that additional care is needed to suppress numerical oscillations away from discontinuities in all types except pure WENO methods. In this paper, a simple explicit (i.e., noncompact) hybrid scheme with such a feature is presented. A spatially fourth-order-accurate MacCormack

DOI: 10.1002/fld

scheme and a SLAU2 scheme [31–34] extended to a higher order using the MUSCL approach are used as components. The hybridization procedure is based on a discontinuity sensor proposed by Genin [35] and a newly devised Gibbs phenomenon detector. In the rest of this paper, the hybridization procedure is first explained and then validated using a variety of canonical problems that have been proposed for testing solvers intended for supersonic turbulence.

2. HYBRID SOLVER

An explicit, second-order Runge–Kutta scheme is used for temporal integration of the governing equations. Second-order temporal accuracy is generally considered adequate for LES. Temporal accuracy can easily be extended to higher orders if needed later.

A cell-centered finite volume scheme is used to spatially discretize the governing equations. The desirable spectral characteristics of the scheme depend on how the inviscid fluxes at the cell face centers are constructed using dependent variables (conservative variables in the present case) at cell centers.

The following expression is used to compute the flux at cell faces:

$$F_h = \theta F_c + (1 - \theta) F_u \tag{1}$$

F_c and F_u are the centered and upwind fluxes computed, respectively, using fourth-order MacCormack and second-order modified SLAU2 schemes. The MacCormack scheme is a good choice because it is perhaps the simplest nondissipative scheme that does not need artificial dissipation for stability or special care like the Rhie–Chow correction [36] for preventing checkerboard-type oscillations on nonstaggered meshes. It was spatially second order accurate originally, but fourth-order versions have been developed later [35, 37, 38]. The spatial stencil proposed by Genin [35], which minimizes the numerical oscillations, is used for interpolation of variables from cell centers to cell faces. Like in the original MacCormack scheme, fluxes in the present work are computed at cell centers and interpolated to the cell faces rather than interpolation of conserved variables to the cell faces and construction of fluxes based on them.

Prior to hybridization, the central scheme has been independently checked for its spatial order of accuracy using the Taylor–Green vortex problem. The details of the scheme and results for this problem are included in Appendix A. Two-dimensional laminar flow in a lid-driven cavity [39] has also been simulated in order to check if grid independence is reached at 80×80 resolution as observed in many previous studies [40]. The details of this exercise are left out here for brevity.

The SLAU2 scheme developed by Shima and Kitamura [32, 33] has recently been modified to improve shock-predicting capability [34]. This scheme has features well suited for DNS and LES. It has robust shock-capturing ability, which is impervious to the specification of the numerical speed of sound. This feature should be very useful in simulating reacting flows in which determining the speed of sound is not easy. It also has numerical dissipation low enough to overcome the D'Alembert paradox that plagues many flux split schemes. This scheme is used here with a van Albada limiter.

θ is the switch that is closer to unity in smooth regions of the flow so that the turbulence dynamics are accurately captured. Near shocks and other discontinuities, θ, tend to zero so that the contribution of the shock-capturing scheme to the overall flux, F_h, dominates and an oscillation-free solution is predicted.

Designing a proper switching function is so critical to the overall performance of hybrid schemes that it has been the focus of many published studies [17, 29, 41–45]. Similar challenges exist for designing other high-resolution shock-capturing methods. Pure WENO schemes need smoothness detectors [15, 16, 46], while artificial diffusivity (hyperdiffusion) methods [9, 10] require carefully designed hyperdiffusivity terms with adjustable constants in order to localize their effects them where needed. A comprehensive review is beyond the scope of this paper, but a noteworthy fact of relevance is that most of switching functions were designed to hybridize compact and ENO/WENO schemes. Hyperdiffusivity approaches are almost always implemented on compact schemes, and so the prescribed numerical constants may also be specific to compact schemes [10]. The one

DOI: 10.1002/fld

exception is the switching function proposed by Genin [35], which was used to hybridize a fourth-order central scheme with a MUSCL-based Riemann solver just as in the present instance. A modified version of it is used here. The Riemann solver used by Genin was a further hybrid between Harten–Lax–van Leer contact (HLLC) [47] and Harten–Lax–van Leer–Einfeldt (HLLE) solvers [48], and so that approach involves two steps of hybridization and is, therefore, significantly more complex than the present approach.

The switching function is based on gradients of pressure and density fields so as to be applicable in handling both shocks and contact discontinuities. The smoothness parameter of a field variable ϕ is defined [35] as follows:

$$\begin{aligned} S_{\phi,i} &= \frac{|\phi_{i+1} - 2\phi_i + \phi_{i-1}|}{|\phi_{i+1} - \phi_i| + |\phi_i - \phi_{i-1}|}, \text{ if } |\phi_{i+1} - 2\phi_i + \phi_{i-1}| \geqslant \epsilon_\phi \phi_i \\ &= -S_\phi^{th}, \text{ otherwise} \end{aligned} \tag{2}$$

The coefficients ϵ_P and ϵ_ρ for pressure and density fields were set to 0.05 and 0.1, respectively, through numerical experimentation in earlier work [35], and the same values are retained here. The threshold values S_P^{th} and S_ρ^{th} equal 0.5 and 0.25, respectively. The overall smoothness parameter at a cell interface between cells (i, j, k) and $(i+1, j, k)$ is determined using smoothness parameters at cell centers.

$$S_{i+1/2} = \max(S_{P,i}, S_{P,i+1}, S_{\rho,i}, S_{\rho,i+1}) \tag{3}$$

Genin [35] used a Heaviside function of smoothness parameter to arrive at the switch (i.e., $\theta_{i+1/2} = 1 - H(S_{i+1/2})$). So, switching between central and flux split schemes was abrupt rather than gradual. This leads to generation of numerical oscillations around sharp fronts although they do not grow to destabilize the simulations as in the case of purely central schemes.

More gradual switching can suppress the oscillations, but some of the physical oscillations are also dissipated in the process. A balance between some unwanted dissipation of physical oscillations and the Gibbs phenomenon is characteristic of almost all switching functions proposed so far. Incidentally, the hyperdiffusivity approaches, which are alternatives to hybrid approaches, also have this problem while determining where exactly and how much hyperdiffusion should be added to suppress numerical oscillations around shocks. The same is true in the case of nonoscillatory schemes as well. The ENO schemes switch between higher-order and lower-order stencils in order to capture both physical fluctuations and sharp fronts. Weights were added later to the stencils to facilitate more gradual switching to arrive at WENO schemes that are now used instead of ENO schemes. When hybridized with compact (or other nondissipative) schemes, not only the procedure for computing weights but also appropriate switching functions and associated constants have to be chosen carefully for desirable results [17, 26].

A modification that helps the hybrid scheme suppress oscillations associated with the Gibbs phenomenon away from discontinuities is made to the switching procedure. In a way, this can be viewed as a simpler alternative to the filtering step used in many other alternate methods discussed previously [13, 14, 49]. This type of filtering is usually based on a very-high-order spatial filter (typically eighth or higher). The proposed modification here is a bit more practical for complex geometries.

The Gibbs phenomenon results in checkerboard-type oscillations. A way to detect these oscillations is to compute a function that characterizes them.

$$S'_{i+1/2} = \frac{(\rho_{i+2} - 2\rho_{i+1} + \rho_i)(\rho_{i+1} - 2\rho_i + \rho_{i-1})}{(\rho_{i+1} - \rho_i)^2} \tag{4}$$

Negative values of S' are indicative of the unphysical Gibbs phenomenon. Earlier, the presence of a local maxima next to a local minima (which is easy to detect using gradient ratios needed for the

DOI: 10.1002/fld

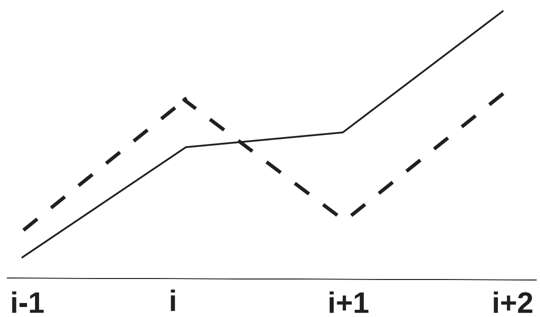

Figure 1. Identification of unphysical oscillations. Both curves are indicative of unphysical two-point oscillations. The dotted line has a local maxima next to a local minima, but the solid line has no local extrema because of a mean gradient. So the presence of local extrema at two consecutive locations is not a necessary condition for unphysical behavior, and this cannot be used as a criterion for identifying unphysical behavior. S' computed as in Equation (4) is negative in both cases, indicating unphysical behavior.

MUSCL procedure) was considered as a way of characterizing unphysical oscillations. Although quite effective, that approach cannot characterize Gibbs phenomenon in the presence of a strong long-range gradient in the density field. The preceding expression, on the other hand, can always detect the Gibbs phenomenon. This is explained using an illustration in Figure 1. To suppress the numerical oscillations, a nonzero weight for the flux split scheme contribution to the overall flux is needed. So, the switching function is now calculated as a function of both S, the shock or contact discontinuity sensor, and S', the Gibbs phenomenon detector.

$$\theta = \min\left[\frac{1}{1+\exp(14S)}, \exp(\min(2.5S', 0.0))\right] \tag{5}$$

The need to include S' in the computation of the switching function is established later by simulating several test problems.

There are adjustable constants involved in determining the weights for combining the two schemes just like in other hybrid schemes. There are such constants in almost all other competing methods as well. Unlike in some illustrative studies [18] that seek to demonstrate the potential of a proposed approach by freely adjusting the constants independently for each test problem or in comparative studies [6, 11] involving the best solutions (obtained using optimal switching functions and associated constants) of various methods for a given problem, the same switching function with fixed constants is used for all the test problems here.

3. RESULTS

The problems to test the present hybrid code are chosen from several past studies. These include the work of Genin and coworkers, which is based on a noncompact hybrid solver much like the present one and which proved to be quite effective for LES of supersonic flows [35, 50] . Some problems in that study were used to test only the shock-capturing scheme and not the final hybrid scheme. In the present study, the hybrid scheme is used for simulating these problems also to ensure that hybridizing with a central scheme does not compromise the shock-capturing ability of the flux split scheme. A comparative study of various high-resolution shock-capturing schemes available at the time by Liska and Wendroff [51] is another prominent study chosen for comparison here.

The test problems fall into two broad categories. The first includes is canonical test cases for high-speed-flow solvers, which do not involve any physical oscillations in solutions. These include one-dimensional and multidimensional flow problems with intense and, in some cases, interacting wave systems. The challenge here is to capture these interactions without creating unphysical oscillations. If a scheme is prone to generating such oscillations, they are clearly evident in isolevel/contour plots,

DOI: 10.1002/fld

especially around shock or contact lines. If there are no physical oscillations that need capturing, traditional shock-capturing schemes extended to second-order accuracy using MUSCL are mostly sufficient for generating reference solutions. Previously published results could also be used for comparison.

The second type of problems have physical oscillations in addition to shocks and other waves. Such oscillations may result from inherent instabilities associated with initial states like in the case of two-dimensional Riemann problems [51] or from the interaction of initial spatial fluctuations with waves in supersonic flows. The Shu–Osher test [52], interaction of a single vortex with a shock wave [46, 53] and shock amplification of a vorticity field [54] are a few problems that are in this category. The physical oscillations have to be captured without creating artificial ones around shock waves. No analytical solutions are available, and so reference solutions are generally obtained using ultra-high-resolution WENO simulations.

3.1. Circular blast wave problem

A two-dimensional explosion test designed by Toro [55] is used to test how well curved shock waves retain their shapes when they are not aligned with the grid [51, 56]. The crispness of the shock structure and extent of post-shock oscillations predicted by a high-resolution solver may depend on the relative alignment of the shock with respect to the mesh orientation. The domain is a square of size 2.0 units with open boundaries. The density and pressure inside a circle of radius 0.4 are both set to 1.0 while they equal 0.125 and 0.1 units, respectively, elsewhere. The gas constant is set to unity. The flow is simulated over a time of 0.25 units on a uniform cartesian mesh just as suggested by Toro [55]. In a way, this problem appears to be a radially symmetric counterpart of the Sod test case [57]. However, it is more complex as pointed out by Toro. The solution has complex interaction between several waves. Initially, it has outward traveling and gradually weakening shock and contact waves and a rarefaction wave traveling inwards towards the center. The contact wave eventually stops and starts traveling inwards while rarefaction reflects from the center and overexpands the flow so as to create an inward-traveling shock.

Some schemes may exhibit numerical oscillations behind shocks as the grid is refined while producing oscillation-free shock and contact line predictions on coarse meshes. So this test was conducted on a quarter of the domain, that too with a highly refined 400×400 mesh by Liska and Wendroff [51] using different schemes. Most of the schemes used in this study may not generate numerical oscillations on a 100×100 grid. Thinner numerical shocks, in general, are more susceptible to instabilities than thicker ones. Flux vector splitting schemes that smear out shock discontinuities are less susceptible to instabilities than flux difference splitting schemes. The challenge of high-resolution shock-capturing comes down to predicting crisp shocks with no post-shock oscillations while retaining contact resolving capability. Difficulties in achieving this has been discussed in many studies, starting from the one published almost two decades ago by Quirk [58].

In the present study, simulations are performed in exactly the same way as reported by Liska and Wendroff [51], and the density isolevel predictions of the SLAU2 and hybrid codes are shown in Figure 2. Just as in their predictions, the pressure fields are quite axisymmetric (not shown here), but density fields are not. Wiggles in density around the contact line are evident in the hybrid code predictions but are relatively benign in comparison with those generated by all the schemes used by Liska and Wendroff [51]. Note that a significant amount of work has been carried out towards improving some of the schemes used in this study (especially the WENO-based ones), and recent versions may provide much better predictions.

One key observation evident from the results of Liska and Wendroff [51] is that more dissipative schemes that smear out shocks and contact lines tend to retain radial symmetry better but are likely to wipe out physical fluctuations (as seen in solutions of other problems). The weighted average flux (WAF)-HLLC scheme of Toro [55] captures the contact line better than others but is prone to wiggles when it is aligned with the grid directions. The high-resolution solvers like WENO and piecewise parabolic method (PPM) also seem to be susceptible to oscillations around the contact line. WENO also predicts wiggles mostly when the contact line is aligned with the grid while PPM has less directional dependence. As mentioned before, higher interpolations along grid lines do not

DOI: 10.1002/fld

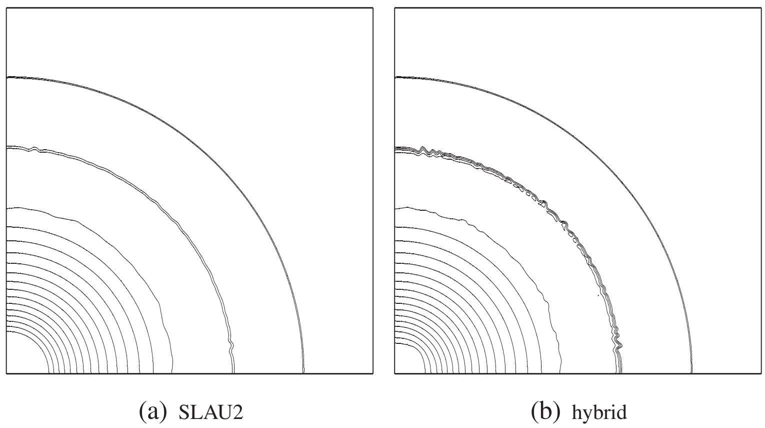

Figure 2. Predicted density isolevels for the circular blast wave problem. Isolevels correspond to 30 uniformly distributed values between minimum and maximum values.

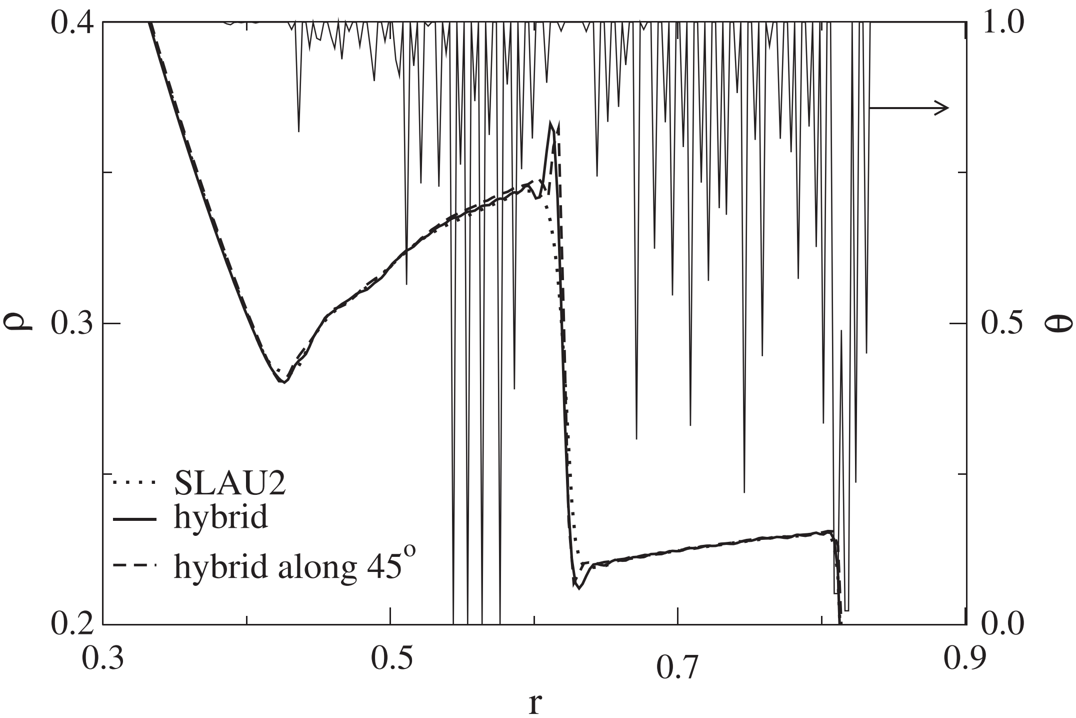

Figure 3. Predicted radial density profiles for the circular blast wave problem.

necessarily guarantee higher-order solutions and may even lead to oscillations in multidimensional flow problems [15, 51, 59]. The hybrid code predicts shock and contact lines as crisply as the high-resolution solvers used by Liska and Wendroff [51] but with much smaller numerical oscillations in density field behind the contact line.

The radial density profiles are plotted in Figure 3 to show the levels of oscillations generated behind wave fronts. Predictions of the hybrid code along the horizontal axis and the 45° line are compared with the SLAU2 prediction along the horizontal axis (the latter matches the reference solution generated using random-choice method [55], but this is not shown here). In addition to Figure 2, this plot illustrates that the hybrid code has minimal directional dependence compared with WAF-HLLC and WENO codes used by Liska and Wendroff [51] and is less prone to unphysical

DOI: 10.1002/fld

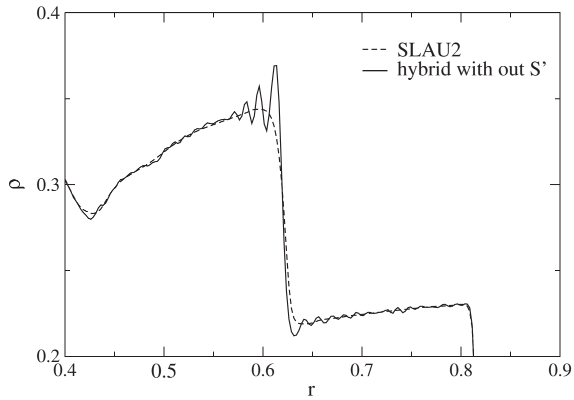

Figure 4. Effect of leaving out the Gibbs phenomenon sensor in determining the weights of the hybrid code.

instabilities around the contact line than the PPM methods. Very-low-amplitude (about 0.4%) post-shock oscillations (located at $r \sim 0.81$) are generated, which persist till the contact line (located at $r \sim 0.62$). The post-contact line oscillations are higher in amplitude (roughly around 12% relative to jump in density across the contact line and not the reference density for the problem) but dissipate quickly behind it. The effect of changing the numerical constants in Equation (5) is briefly discussed in Appendix B.

The radial variation of θ (the switching/blending function) when using the hybrid scheme is also plotted in Figure 3 using a different vertical axis on the right. The SLAU2 scheme has non-zero contributions even at locations away from the shock and the contact line. θ variation is found to be highly oscillatory. Although this is not the case in most of the other test problems, this fact remains a point of concern. It is to be noted in this context that the hyperviscosity approach [8] has a similar problem. The hyperviscosity computed using higher-order polyharmonic operators can become too large near discontinuities. The filtering operation to get around this problem has been reported to result in high-wavenumber variations in hyperviscosity.

When the unphysical oscillation sensor is not considered in determining the weights, the oscillations seem to persist for much longer distances. This is demonstrated by using the shock/contact line sensor alone and leaving out the Gibbs phenomenon detector in determining the weights for the hybrid code and comparing its results with those of SLAU2 in Figure 4. The consequences of using the Gibbs phenomenon detector are surprising given that the numerical oscillations that are removed by using it are not the two-point sawtooth-like oscillations that it is designed to control. It also seems to remove oscillations of longer wavelengths. One likely explanation is the following. The central flux in the hybrid code generates two-point oscillations, and the hybrid code, in turn, generates the higher-wavelength fluctuations as a response. Effective control of two-point oscillations seems to suppress both.

When unphysical oscillations generated at sharp fronts propagate far away, it is generally very difficult to control them. This is partly because they cannot be characterized well in physical space. Often, damping (in the form of artificial dissipation or that associated with a dissipative scheme) is localized around a discontinuity using a discontinuity sensor. If the distance between the location of oscillations and the discontinuity is beyond the half-width of the spatial stencil, a localized damping approach does not work. Either higher-order WENO schemes with large stencils or an additional filtering step [14, 60] is commonly used to effectively suppress numerical oscillations. The use of a Gibbs phenomenon sensor either localizes overall dissipation and prevents the spurious oscillations from propagating far away like in the former or kills the oscillations even far away from discontinuities like in the latter.

The previously published [51] and present results for this problem highlight an important observation regarding high-resolution solvers for supersonic flows. Often, much attention is paid to capturing shocks accurately while developing the solvers, and so they may end up developing problems around contact discontinuities. The same seems to be true in the case of the present scheme

DOI: 10.1002/fld

as well. A similar behavior was shown by Pirozzoli [6] for higher-order compact–WENO hybrid schemes when applied to a two-dimensional Riemann problem involving shock diffraction. Shocks were well captured, but oscillations seem to appear around contact lines.

3.2. Supersonic flow around a cylinder

This case was chosen to verify if the hybrid solver can capture a curved shock without generating unphysical wiggles. Only a few studies [9, 30, 46, 61], to the authors' knowledge, have considered this test problem. It is not usually considered a test case for LES solvers because there are no physical oscillations that need capturing. But unphysical wiggles may be generated just as in the case of Toro's blast wave problem discussed earlier. This problem is considered in addition to the blast wave problem due to two key differences. The shock unlike in the blast wave problem is stationary, and its alignment with the flow covers a range of values. The shock is always normal to the flow in the blast wave problem.

Fiorina and Lele [9] simulated a Mach 3 flow around a cylinder using a solver based on hyperdiffusivity approach. The curvilinear grid with radial and circumferential lines was orthogonal with zero skewness. The pressure isolevels predicted by the hybrid solver for this problem on a mesh identical to theirs is shown in Figure 5. The present method seems to suppress the post-shock unphysical kinks in pressure better than the hyperdiffusivity approach. It is also to be noted that abrupt switching between the two schemes generates numerical oscillations that destabilize this simulation. Gradual switching and the unphysical oscillation sensor are highly necessary for this case.

Tu and Yuan [30] simulated a Mach 4 flow around a cylinder using a characteristic filtering-based compact scheme and a nonorthogonal grid. A nonorthogonal grid of the same size (60×60) generated by compressing an orthogonal grid (with radial and circumferential lines) in the flow direction by a factor of 0.4 is used here for simulating the same flow here. The density fields predicted using the hybrid scheme are shown in Figure 6. Two differences are evident when this figure is compared with the corresponding plot of Tu and Yuan [30]. Shock thickness is higher in the case of the present hybrid solver, which is expected because of the use of SLAU2, a scheme that is known to predict thicker shocks than flux difference splitting schemes as well as other advection upstream splitting method (AUSM) variants. The difference is not so stark when the present solution is compared

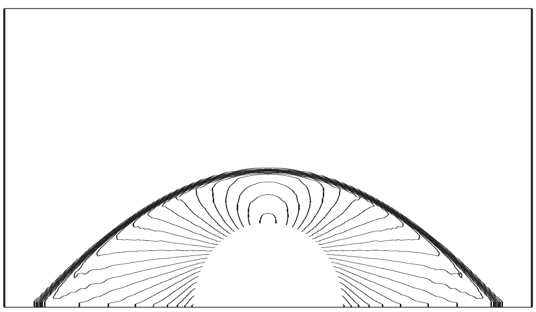

Figure 5. Pressure isolevels for Mach 3 flow past a circular cylinder predicted using the present hybrid scheme. Isolevels correspond to 30 uniformly distributed values between minimum and maximum pressures.

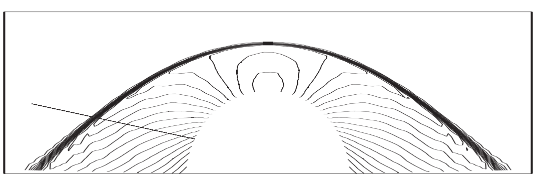

Figure 6. Density isolevels (corresponding to 20 uniformly distributed values between minimum and maximum values) for Mach 4 flow around a circular cylinder predicted using the present hybrid scheme. A grid line shown in the figure so that density variation along it could be compared with a reference solution.

DOI: 10.1002/fld

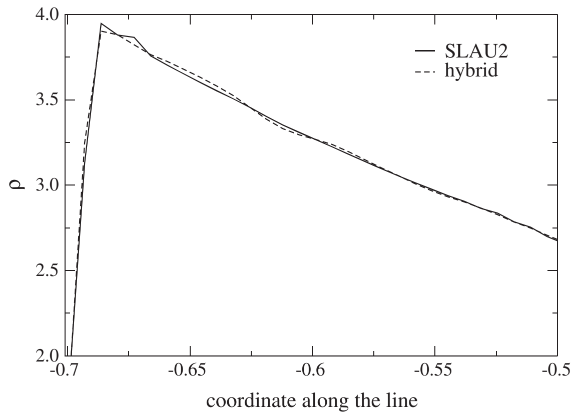

Figure 7. Comparison of density predictions along a grid line (shown in Figure 6).

with the one obtained using WENO on a similar nonorthogonal grid by Shu [61] (although Shu's result [61] corresponds to a freestream Mach number of 3 and only pressure isolevels were provided). Compared with the predictions of the hybrid solver, the shock thickness in these studies did not change as drastically, as one moves away from the centerline. This is because WENO [61] and upwind characteristic filtering [30] provide better shock-resolving capability than the second-order MUSCL scheme used here for the purpose.

No post-shock oscillations are predicted when the normal to the shock is aligned with the flow direction, but as the angle between them increases, unlike in the prediction of Tu and Yuan [30], slight post-shock oscillations are evident. No such oscillations are predicted behind a straight oblique shock (while predicting flow past a wedge). So these oscillations seem to a consequence of shock curvature rather than its relative alignment with the flow direction.

When predictions of the hybrid code and SLAU2 are compared, the pressure fields (isolevel plots) were indistinguishable visually while the density field in the case of the hybrid scheme seems to have very mild wiggles. The maximum amplitude of the wiggles in the density field is below the 2% level. For comparison, Fiorina and Lele [9] reported wiggles in the pressure field of about 2% amplitude for a Mach 3 test case. Compared with the theoretical value, a hybrid code underpredicts the stagnation point density (the maximum value of density) by 0.8%.

Along a (grid) line shown in Figure 6, the predictions of density by SLAU2 and hybrid codes are compared in Figure 7. The maximum difference in predictions along this line is about 1.2%. Note that the plot shows that MUSCL fails to keep the SLAU2 solution monotone. The hybrid code relies on the shock-capturing scheme to keep unphysical oscillations around the shock in check. If the latter itself predicts nonmonotone solutions, the problem of numerical oscillations may be further exacerbated by the central scheme, which has a nonzero weight behind the shock. In the future, a multidimensional limiter could be considered for extending SLAU2 to the second order, and using that may also improve the hybrid code predictions.

3.3. Emery test

This test introduced by Emery [62] and used extensively in many later studies involves unsteady supersonic flow over a forward-facing step. Specifically, the Mach number everywhere initially in a 3×1 domain is set to 3.0. Then, a step of height 0.2 that begins at axial length 0.6 from the upstream end and extends all the way to the downstream end is introduced suddenly at zero time. After integrating for a fixed amount of time, the solution is examined for signs of unphysical behavior and accuracy.

The density isolevels predicted by both hybrid and flux split schemes using a 240×80 mesh are compared in Figure 8. The corner entropy fix suggested by Woodward and Colella [63] was used at the expansion corner to prevent the numerical boundary layer downstream that most schemes produce. The hybrid code predicts the shocks almost as well as the pure flux split scheme. There

DOI: 10.1002/fld

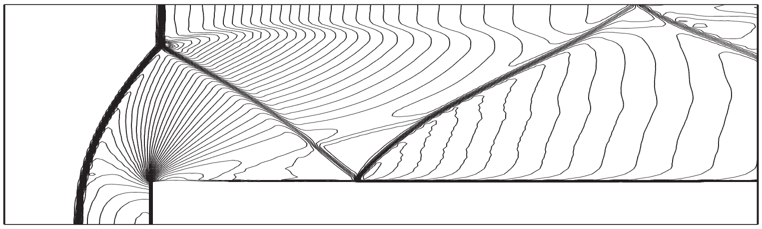

(a) SLAU2

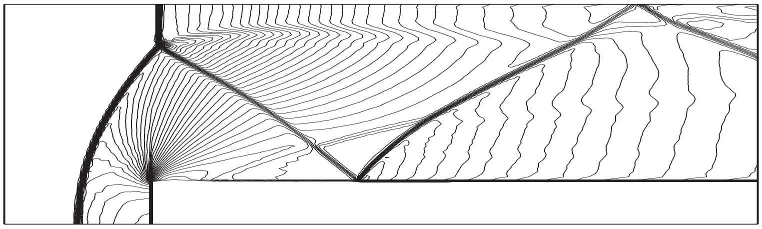

(b) hybrid

Figure 8. Density isolevels for the Emery test problem.

appears to be no unphysical behavior at the triple point, and the crispness of the contact line originating at that point is better in the case of the hybrid scheme and is on par with the best of contact resolving schemes. Except for a bit thicker shocks resulting from the use of SLAU2 for shock capturing, the present hybrid solver predictions are on par with those of fourth-order ENO and fifth-order WENO schemes [46].

The effects of the slip line generated at the concave corner seem to remain even after it crosses both the shocks incident and reflected off the lower wall. This is evident from the hybrid-code-predicted density isolevels downstream of the shock reflected from the bottom wall (at an axial location roughly midway between inflow and outflow boundaries). The hybrid code captures this feature as well as the fifth-order WENO scheme and better than the fourth-order ENO scheme [46]. There is very little hint of it in the predictions of the more dissipative, second-order-accurate SLAU2 scheme.

3.4. Shu–Osher test

This one-dimensional test involves a Mach 3 shock wave moving through a sinusoidally varying density/entropy field. The shock amplifies the oscillations as it passes through. No analytical solution is available, and so reference solution is usually generated using a WENO scheme on a highly refined mesh.

The initial flow field is specified as follows. On a [0:10] domain, a Mach 3 shock is located at $x = 2$. The conditions behind the shock are determined using moving normal shock relations by assuming unit values for pressure and density ahead of the shock. The density ahead of the shock is perturbed sinusoidally as follows.

$$\rho = 1 + 0.2\sin(5x) \tag{6}$$

The left boundary has supersonic inflow, and at the right boundary, the flow is stagnant, and the pressure is locally uniform during the course of the simulation. So, the initial state is maintained at the right boundary. Integration is performed over a time of 1.872, and then solutions are compared with reference solutions.

Generally, a code is considered acceptable for capturing supersonic turbulence if the dynamics can be captured well on mesh with 400 points [18, 30, 35, 51, 64, 65]. So, this resolution is used here as well. Artificial diffusivity-based methods [8, 11] seem capable of capturing the physical oscillations

DOI: 10.1002/fld

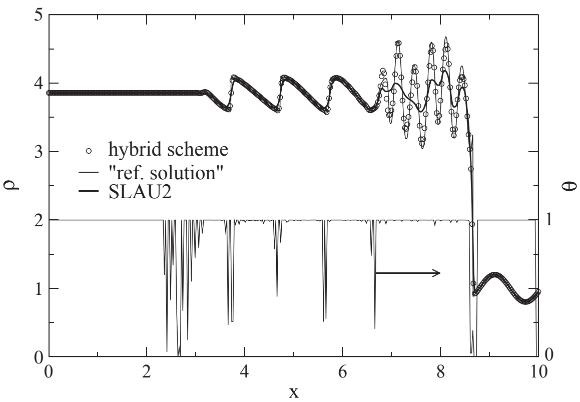

Figure 9. Prediction of density field for the Shu–Osher problem using the present hybrid scheme.

immediately behind the primary moving shock with just 200 points. However, the shocklets that form behind the primary shock wave as the compression waves collapse are more smeared, and there is a rather large kink in the density field at the left edge of the sinusoidal fluctuations. It is to be noted that the capturing of the physical fluctuations with fewer grid points in artificial diffusivity methods [8, 11] is due to the use of compact schemes. In fact, the results from these studies could not be replicated in the present study when the same artificial diffusivity models were used with the present fourth-order central scheme. The compact schemes are usually of higher order (sixth usually), and proper design of artificial diffusivity renders them with high resolution as well. The design seems to be specific to the compact schemes. The distinction between resolution and formal order of accuracy was explained by Adams and Shariff [18] and demonstrated using this very problem by Pirozzoli [19].

The density field predicted by the hybrid code is compared with the reference solution in Figure 9. The physical oscillations are captured well without any numerical artifacts. There is a small kink in the density profile at the upstream end of the oscillations (which is more visible in the next figure), but it is relatively insignificant compared with one generated by the artificial diffusivity-based methods [8, 11].

Note that SLAU2 was designed to minimize the numerical dissipation in order to overcome the D'Alembert paradox [33]. Its damping of kinetic energy and vorticity are, therefore, lower than those of almost all other flux split schemes. In terms of damping density fluctuations (which are a key feature of highly compressible turbulence), as seen in Figure 9, it is comparable with other flux split schemes. A likely explanation is that not all the characteristic waves associated with Euler equations are affected the same way by the SLAU2 construction. The damping of entropy wave seems just as high as in case of other Riemann solvers. This observation highlights the need for a hybrid scheme despite the fact that SLAU2 has many features desirable in DNS/LES solvers (as explained earlier).

Also shown in Figure 9 is the variation of θ in space. It is clear that the central scheme is dominant for the most part and the SLAU2 contribution is needed only around the primary shock wave and the compression waves that collapse into shocklets. To the left of the point where density fluctuations begin, unphysical oscillations are detected, and SLAU2 contribution seems necessary.

The need for a switching function that facilitates gradual rather than abrupt switching based on not only a discontinuity sensor but also an unphysical oscillation sensor is established in Figure 10. On a scale similar to one for Figure 9, the predictions made with and without the unphysical oscillation sensor are quite similar, and so this plot uses a different scale to highlight the differences. Although the spurious oscillations resulting from abrupt switching are reduced by resorting to more gradual switching, the amplitudes are still unacceptable. Even more gradual switching can reduce these oscillations, but the increased damping would also damp out the physical density/entropy oscillations. This is demonstrated in Appendix B. Constructing a switching function that also depends on an unphysical oscillation sensor would selectively suppress only the spurious/numerical oscillations, is a better alternative as evident from Figure 10. As noted earlier, the

DOI: 10.1002/fld

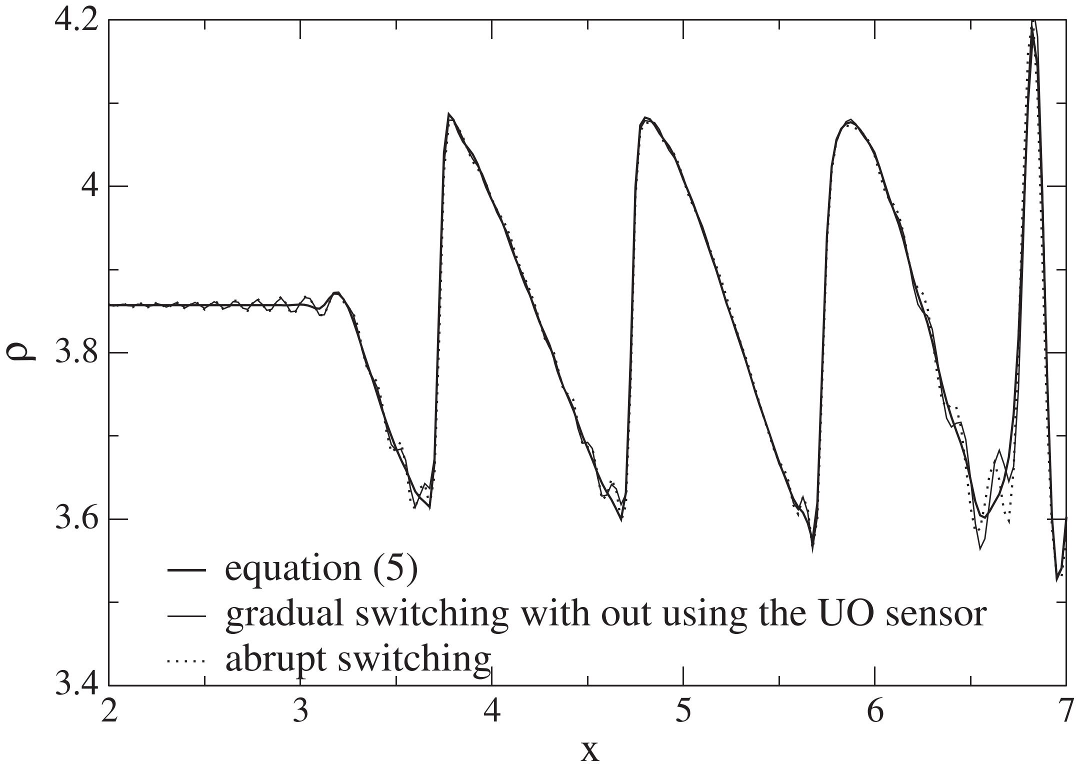

Figure 10. Effects of gradual switching between the schemes and the unphysical oscillation sensor.

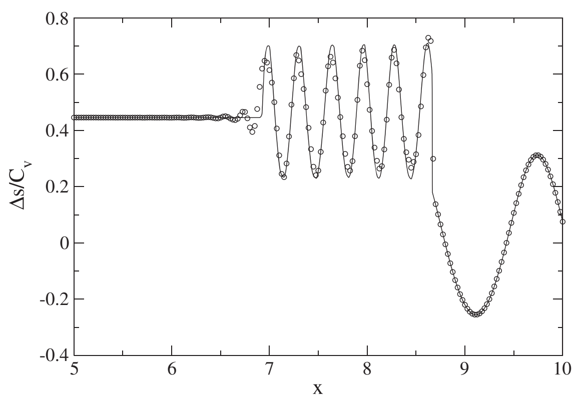

Figure 11. Entropy profiles for the Shu–Osher test problem.

SLAU2 contribution seems necessary just to the left of where the physical oscillations begin. Even though these spurious oscillations are not two-point oscillations, they are suppressed quite effectively. It is precisely at the starting point of the oscillations where the hyperviscosity approaches (which otherwise work well for this problem) create a rather large unphysical kink in the density field. The small kink resulting from the hybrid code evident in this figure is much smaller in comparison.

Density variations shown in previous plots result from acoustic and entropy waves behind the moving primary shock wave. The numerical dissipation associated with any scheme is directly correlated to how well it captures entropy waves. Difference between various schemes can be most prominently seen by looking at entropy fluctuations [11]. Figure 11 shows the predicted profile of entropy change (over reference state) nondimensionalized by specific heat at constant volume.

DOI: 10.1002/fld

When compared with the reference solution, it is clear that the numerical dissipation is slightly more than in the compact–ENO hybrid of Adams and Shariff [18]. Johnsen and coworkers [11] presented similar plots for various schemes, but for simulations performed with half the number of grid points. The numerical dissipation associated with WENO and shock fit methods seems to be quite high even in smooth regions of the flow (away from the shock) while that of compact schemes with hyperdiffusivity is acceptable. The level of dissipation of the present hybrid is even lower albeit at double the resolution used in compact schemes.

3.5. Shock–vortex interaction

Formulated originally by Shu [46, 53] and used in several later studies [14, 30], this test involves convecting a compressible isentropic vortex through a stationary Mach 1.1 normal shock located at $x = 0.5$ in a $[0, 2] \times [0, 1]$ domain. The conditions behind the shock are obtained using Rankine–Hugonoit relations. The gas constant, reference nondimensional pressure and density are all set to unity. A small compressible vortex centered initially at $[0.25, 0.5]$ and perturbs the velocity, temperature and entropy fields according the following equations is convected by the incoming flow into the shock.

$$u' = \epsilon\tau e^{\alpha(1-\tau^2)}\sin\theta \tag{7}$$

$$v' = -\epsilon\tau e^{\alpha(1-\tau^2)}\cos\theta \tag{8}$$

$$T' = -\frac{(\gamma-1)\epsilon^2 e^{2\alpha(1-\tau^2)}}{4\alpha\gamma} \tag{9}$$

$$S' = 0 \tag{10}$$

where τ is the distance from the center of the vortex nondimensionalized by the critical radius of the vortex, which equals 0.05. The parameters $\alpha = 0.204$ and $\epsilon = 0.3$ quantify the radial spread and intensity of the vortex. The preceding equations represent a steady-state solution of Euler equations. Reflective boundary conditions are used at the top and bottom boundaries. The simulations are usually performed till the vortex crosses the shock almost completely at a time of 0.35 s.

Before simulating the shock vortex interaction, the very long-term evolution of the vortex was simulated to assess the damping of the hybrid scheme just as in some previous studies [15, 29, 61]. Negligible damping was seen after a time of 10 while it was noticeable after a time of 40. Unlike the WENO scheme designed by Shu [61] or the higher-order artificial compression methods (ACM) of Yee and coworkers [29], the present method could not maintain an indefinite undamped state, but the solution turns out to be much better than the one obtained using the total variation diminishing (TVD) filter reported by Yee and coworkers [29]. Although the central scheme is expected to be used in the absence of shocks, the slow decay is explained as follows. The central schemes generate very low-level density fluctuations. When the solver interprets them as unphysical (as per Equation (4)), the weight associated with the flux split scheme becomes nonzero, and this contributes to some dissipation. This additional dissipation has to be weighed against the advantage this scheme offers by preventing the Gibbs phenomenon around strong gradients.

Shu [46] used a very early version of the WENO scheme and a 250×100 mesh that was uniform in the lateral direction and clustered around the shock in the axial direction. Lo and coworkers [14] used a similar mesh and a compact scheme stabilized with characteristic filtering. They used both global and localized versions of TVD, MUSCL, and WENO filters in a comparative study. Local filtering generally resulted in better solutions (i.e., without numerical oscillations around shocks and low dissipation far away from shocks), especially in the cases of TVD and MUSCL. But localization required shock detection, which was carried out using a Ducros sensor [43] for TVD and MUSCL,

DOI: 10.1002/fld

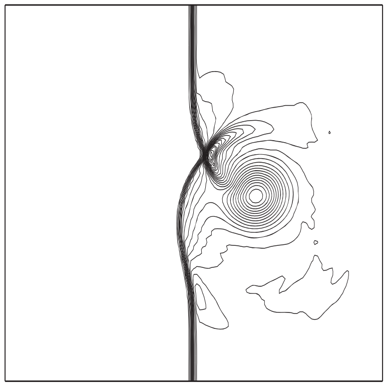

Figure 12. Pressure isolevels (corresponding to 30 uniformly placed values between the minimum and maximum) during shock vortex interaction predicted using the present hybrid scheme.

while a WENO smoothness indicator was used in the case of WENO. Tu and Yuan [30] used a 200×100 mesh, but it was uniform in both directions. Their method was also based on a compact scheme, but it was upwinded unlike the central version of Lo *et al.* [14]. Characteristic-based flux limiting (somewhat similar to the characteristic filtering of Lo *et al.*) was used to control oscillations generated by the compact scheme around the shocks.

The studies of Lo *et al.* [14] and Tu *et al.* [30] provided the reference solutions for comparison here. Key differences are to be noted prior to the comparison. A 250×100 grid that is uniform in both directions was used here. Also, Lo *et al.* [14] did not use the same values of parameters associated with shock detection for all test problems. Optimal values were presumably chosen to arrive at the best possible solution in each case. That makes sense in a comparative study. Such problem-specific tuning was not resorted to here. Tu and Yuan [30] reported using a single user-specified parameter, but it was to avoid division by zero, and results remained insensitive to it. Like in the present case, there was no problem-specific adjustment.

The pressure isolevels from the present study in Figure 12 compare well (barring the outlying contours at outer edges of the vortex that are affected by numerical noise) with the corresponding predictions of Tu *et al.* [30] and the local WENO filter-based prediction of Lo *et al.* [14]. The shock resolution by Lo *et al.* [14] is better owing to grid clustering around the shock. The present scheme does not generate any numerical oscillations of the kind observed in their predictions [14] made using global TVD or MUSCL filters. An example of improper damping that may result in numerical oscillations around the shocks can be seen in the results of Lo *et al.* [14] obtained using MUSCL-based characteristic filtering. It is interesting to note that the present shock-capturing scheme is extended to the second order using MUSCL and hybridized with a central scheme, but it does not produce similar kind of oscillations.

4. SHOCK INTERACTION WITH VORTICITY FIELD

This test involves interactions of Mach 8 (with a much higher intensity than in the case of shock–vortex interaction test) with a two-dimensional vorticity field. First proposed by Zang *et al.* [54] for testing numerical methods ability to capture turbulence amplification through shocks and used in the seminal work on ENO schemes by Shu *et al.* [52], it has been used to test codes based on ENO and WENO (pure or hybrid forms) meant for performing LES (e.g., [18, 19, 65, 66]). It is to be noted here that this test was used to compare pure WENO, hybrid and hyperdiffusivity methods by Johnsen *et al.* [11] relatively recently. But they used a much weaker Mach 1.5 shock wave. They concluded that post-shock oscillations were effectively controlled by shock-fitting methods while all shock-capturing methods suffered from post-shock oscillations. Hyperdiffusivity methods produced oscillations of significantly higher amplitudes, which persisted for longer distances behind shocks than the WENO and characteristic filter-based methods.

DOI: 10.1002/fld

A normal shock wave initially located at $x = -1$ location in $[-1.5, 1.5] \times [-1, 1]$ propagates to the right into a flow field with unit values for pressure, density, and velocity variation defined as follows.

$$u = -\sqrt{\gamma} \sin(\pi/6) \cos(2\pi x \cos(\pi/6) + 2\pi y \sin(\pi/6)) \tag{11}$$

$$v = \sqrt{\gamma} \cos(\pi/6) \cos(2\pi x \cos(\pi/6) + 2\pi y \sin(\pi/6)) \tag{12}$$

The vorticity wave is inclined at an angle of $\pi/6$ to the incoming shock wave. The initial state behind the shock is computed from normal shock relations assuming uniform flow ahead of it. Left and right boundaries are held at steady state while periodic boundary conditions are used in the vertical direction. Integration over a time of 0.2 units is performed before solution is compared with a 'reference' solution, which (as usual for problems without analytical solutions) is computed using a very-high-resolution 960×640 uniform mesh.

The physics of the flow has been explained based on the reference solution computed using a very fine mesh by Pirozzoli [19]. The fast-moving acoustic waves are separated by a sharp interface (located roughly at $x = 0.5$) from slower vorticity and entropy waves. The longer-wavelength acoustic dynamics can be captured well using a relatively coarse 60×40 mesh [66]. Even a dissipative TVD scheme seems able to resolve these dynamics. The near-shock behavior poses a real challenge to the solvers. No significant improvement in prediction of this behavior was reported by Hannappel [66] when mesh was refined fourfold in each direction while retaining the TVD scheme. Their study and one by Adams *et al.* [18] focused on establishing the superiority of ENO schemes over dissipative TVD/MUSCL schemes. In fact, performance in the latter was judged based on comparison of predictions with linear theory for shock amplification of vorticity rather than a reference solution. Resolution needed to capture all the features with sufficient accuracy was never established in these studies. Later studies [19, 65] showed that a 192×128 mesh is needed. Even seventh-order WENO or compact–WENO hybrid schemes could not capture the behavior well enough with half this resolution (i.e., a 96×64 grid). With a 192×128, Ghosh [65] reported that both fifth-order WENO and its compact reconstructed version produced similar results. On the other hand, the fifth-order WENO scheme of Pirozzoli [19] was found to be inadequate. It had to be hybridized with a compact scheme.

The density variations along the centerline predicted by the present hybrid scheme and the compact–WENO hybrid are compared with reference high-resolution solutions in Figure 13. Surprisingly, the solutions of Pirozzoli [19] and Ghosh [65] predicted using a 192×128 mesh were quite similar (so only one is shown), but their reference high-resolution solutions differed. It turns out that the solutions are very sensitive to how the shock structure is initialized. The proper way to do this is to solve a steady-state problem to arrive at the normal shock structure and then use the solution to initialize the moving shock. Often, this is not performed. Rather, it is initialized as a

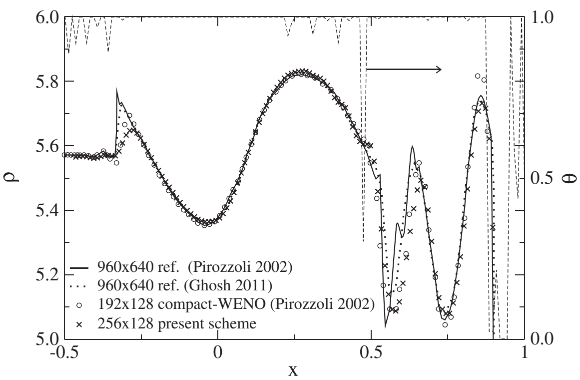

Figure 13. Density variation along the centerline for shock–vorticity interaction problem.

DOI: 10.1002/fld

thin front captured over one grid point. In the process of settling down (i.e., being captured over a few grid points), a weak entropy wave may be generated that travels behind the shock wave as the solution evolves (additional vorticity wave may also be generated if the shock happens to be curved). The amplitude and wavelength of this entropy wave depend on the flux calculation method and the reconstruction procedure used for higher-order extension. More dissipative schemes may dissipate this wave while others will retain it and corrupt the solution. The kinks in density field around $x = 0.6$ in the reference solution of Pirozzoli is a consequence of such corruption. Entropy waves move at the local convective speed, and this location is where an entropy wave coincident with the initial shock wave would be after a time of 0.2 units. A high-resolution simulation with a 720×480 grid and the second-order-accurate SLAU2 (flux split) scheme confirm this assertion. While this solver was not expected to provide a reference solution (owing to its high numerical dissipation) at this resolution, this exercise does confirm that shock initialization as a sharp interface created similar kinks in density field near this location while a proper initialization as explained earlier does not. The results of this exercise have been left out here for brevity.

The solutions to this problem are also sensitive to the numerical shock structure that is a characteristic of the scheme. Small-scale dynamics are not captured in the case of thicker numerical shocks. SLAU2 produces slightly thicker shocks than flux difference splitting schemes (such as one used by Adams [18]) and some of the other shock-capturing schemes including other AUSM variants. Some of the small-scale oscillations are missed if a 192×128 mesh is used. Shock needed to be captured more crisply in order to capture them. So, the resolution was refined by 25% in the shock normal direction in order to obtain solutions on par with those reported by compact–ENO combinations [19, 65]. The θ variation in Figure 13 indicates that unphysical oscillations are generated mostly behind the density interfaces (roughly around $x = -0.35$ and $x = 0.5$) and not as much behind a rather strong shock wave at $x = 0.8$. As noted previously, this points to the need for an increased focus on capturing contact line while constructing high-resolution solvers.

Figure 14 shows the density isolevels predicted by the present hybrid scheme. The interface separating acoustic and entropy/vorticity waves is captured as well as in these earlier studies (albeit at a slightly lower resolution) but better than in the case of the fifth-order pure WENO scheme of Pirozzoli [19]. The hybrid code predicts a small but observable unphysical jump in density just to the left of this interface around $x = 0.5$ (also evident from a careful observation of Figure 13). This is similar to the near contact line jump in the density seen in the hybrid code predictions for a circular blast wave problem. Results of the Emery test indicate no such jumps if the contact line is aligned with the flow. It appears only when the contact line is normal to the flow. The use of unphysical oscillation sensor in determining the weights for the two fluxes in the hybrid scheme localizes this jump without leading to oscillations downstream as demonstrated using the blast wave problem.

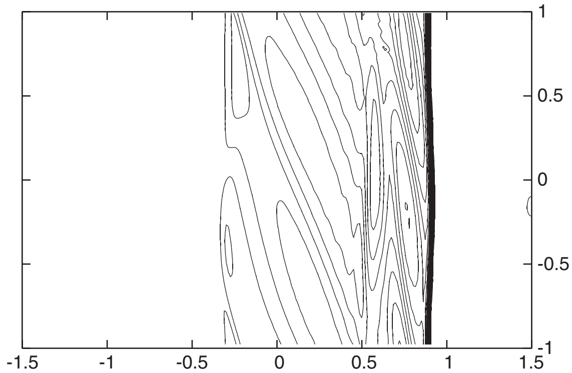

Figure 14. Thirty-four equally placed density isolevels for shock–vorticity interaction problem.

DOI: 10.1002/fld

4.1. Vortex pairing in a temporal mixing layer

This test case introduced by Sandham and coworkers [67] and used in several subsequent studies (e.g., [12, 29]) involves simulating growth and pairing of vortices in a temporal evolving mixing layer at a convective Mach number of 0.8. This Mach is high enough to realize compressible effects on mixing. Compression waves around the vortices collapse into shocklets that are typically found in flows with high, turbulent Mach numbers. To be useful for compressible turbulence, a code has to localize dissipation well enough to capture these shocklets without creating numerical oscillations in their vicinity. Excessive damping away from the shocks may slow the growth of initial instability and delay the roll-up and pairing processes.

A $[0, 30] \times [-50, 50]$ domain is discretized using a 100×100 mesh that is uniform along the abscissa and is clustered at the center in the ordinate direction according to the following mapping.

$$y = 50\frac{\sinh[b_y(y/50)]}{\sinh[b_y]} \tag{13}$$

The velocity field is initialized using a hyperbolic tangent profile.

$$u = \frac{1}{2}\tanh(2y) \tag{14}$$

The velocity jump across the shear layer and the initial vorticity thickness (ratio of velocity jump and maximum velocity gradient) are used as reference velocity and length scales. The normalized temperature is determined by assuming stagnation enthalpy is gradient free. The Reynolds number based on reference quantities is set to 1000.

Functions that approximate eigenmodes [29] for linear growth of instabilities in mixing layers are used to provide initial perturbation to start the roll-up process.

$$v' = \Sigma_1^2 a_k \cos(2\pi k x/30 + \phi_k)\exp(-y^2/b) \tag{15}$$

b, the modulation parameter, is set to 10. The subharmonic ($k = 1$) and most unstable ($k = 2$) waves are triggered by setting their amplitudes to 0.01 and 0.05, respectively. The phase of $-\pi/2$ is used for both waves. The u-velocity perturbation is computed by assuming that the velocity perturbation is divergence free. Periodic and slip boundary conditions are used, respectively, in axial and transverse directions.

Yee and coworkers [29] reported that temperature contours are most sensitive to oscillations and used temperature isolevel plots to analyze their results for this problem. The same is carried out here in Figure 15.

Yee and coworkers [29] simulated this problem at the same resolution using central schemes with characteristic filtering. TVD filtering added too much dissipation, and so increasing the order of the baseline scheme from second all the way to sixth had no effects on the predictions. The roll-up and pairing were delayed, and shock was much thicker when compared with predictions made after adding ACM. The overall evolution of the temperature field here compares well with that predicted with their ACM/TVD filter. Specifically, the results are closer to their so-called ACM44 scheme, which is overall spatially fourth order accurate. The shocks are captured without any numerical oscillations, and the numerical dissipation away from shocks also seems minimal. The parameter κ, which premultiplies the Harten switch in the filtering step, is claimed to be problem dependent in their work [29]. The best results were presumably obtained by adjusting this parameter.

Finally, the consequence of not leaving out the unphysical oscillation sensor while determining the switching function on solution for this problem is illustrated in Figure 16. When the switching is based only on the discontinuity sensor, much numerical noise is generated, and the large-scale structure is also affected. The solution, unlike one generated by considering both the discontinuity and unphysical oscillation sensors, ends up being very different from the one resulting from the ACM44 scheme of Yee and coworkers [29] (which is treated as a reference solution here).

DOI: 10.1002/fld

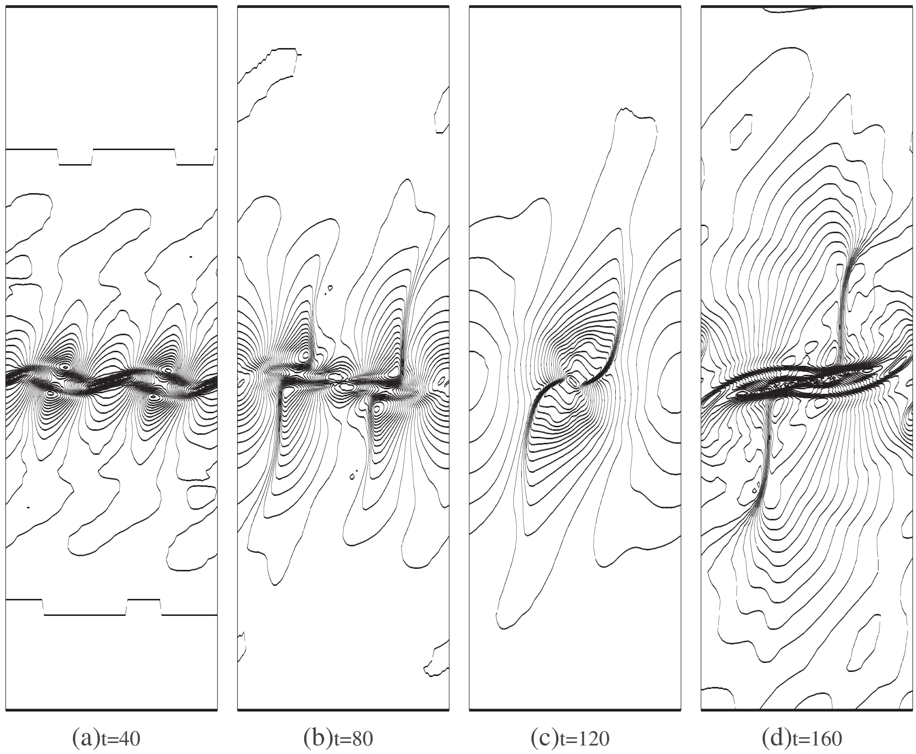

Figure 15. Predicted temperature isolevels during vortex pairing in a mixing layer.

5. CONCLUSIONS

A simple hybrid finite volume method for supersonic turbulence computations has been presented in this paper. The hybrid flux is computed as a weighted average of the spatially fourth-order MacCormack scheme (assuming the error associated with dimensional splitting is negligible) and a second-order SLAU2 scheme developed recently [33, 34]. The method is fully explicit and has a five-point stencil in each direction, the minimum necessary for proper resolution of turbulence. It is highly suited for parallel computing on machines with distributed-memory architecture with just two layers of message passing at block interfaces. The procedure for combining the two schemes differs from those used in the past in that it is based on not only the presence of discontinuities but also spurious unphysical oscillations. Through this procedure, poorly resolved waves are suppressed as suggested by Adams and Shariff [18] without resorting to an additional filtering step [10, 13, 14, 44, 60].

The proposed method captures shocks as well as the SLAU2 scheme with no observable post-shock oscillations in all except the case of inviscid flow around a cylinder. For that problem, the SLAU2 scheme itself produces a nonmonotone solution. It remains to be seen if the hybrid code predictions can be rectified by using a multidimensional limiter instead of the one-dimensional MUSCL procedure for extending the shock-capturing scheme to the second order. The method does produce slight overshoots around contact discontinuities if they are normal to the flow direction. Spurious oscillations that may result from these overshoots are effectively suppressed through the use of a Gibbs phenomenon detector in computing the weights for combining the two fluxes.

The results for the test problems indicate that the resolution of physical oscillations (turbulence) in the present method is on par with fifth-order WENO schemes and only marginally lower than that of compact scheme-based methods. The easier parallelizability and avoidance of an explicit low-pass filtering step can offset this disadvantage while performing DNS or LES of supersonic turbulence.

DOI: 10.1002/fld

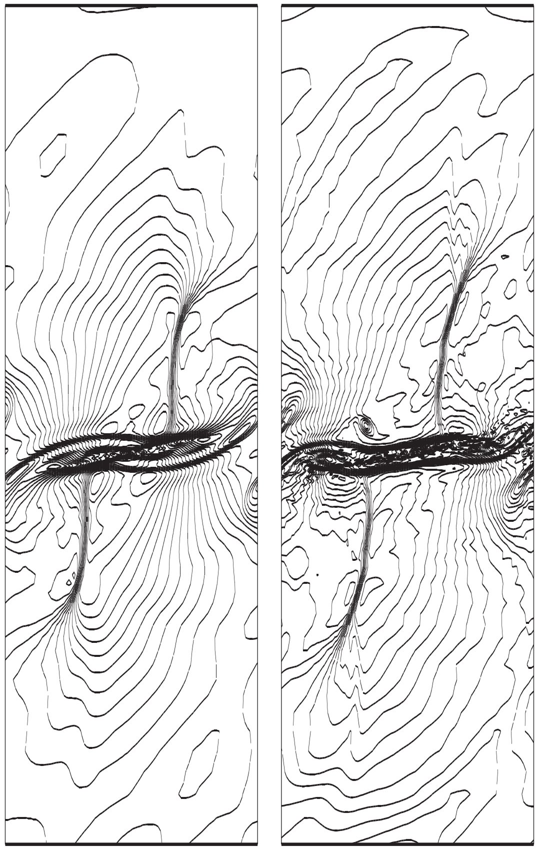
(a)with (b)without

Figure 16. Effect of using the unphysical oscillation sensor for determining the switching function.

APPENDIX A: ORDER OF ACCURACY TEST FOR THE CENTRAL SCHEME

Taylor–Green vortex in the incompressible limit has the following analytical solution.

$$u = \sin(x)\cos(y)e^{-2\nu t} \tag{A.1}$$

$$v = -\cos(x)\sin(y)e^{-2\nu t} \tag{A.2}$$

$$p = \frac{\rho}{4}\left[\cos(2x) + \cos(2y)\right] e^{-4\nu t} \tag{A.3}$$

The flow is periodic in the domain $[0 : 2\pi, 0 : 2\pi]$. The flow is simulated using a 16×16 mesh, and gradually, the resolution is doubled till a mesh of 128×128 is reached. The flow's Reynolds number based on domain size and maximum flow velocity is set to 100. This is typically the value used for validating codes in reported literature. Cell Reynolds number varies between about unity and 6, which is typical of DNS/LES. After significant vortex decay, the maximum error in velocity is computed and plotted against resolution on a logarithmic scale in Figure A.1. A linear fit to the plot has a slope of -3.58, which is reasonably close to -4, which is expected of a fourth-order scheme. If the data point corresponding to the highest resolution is removed, the slope, indeed, is closer to -4, indicating the possibility that machine error may have affected results at this resolution.

DOI: 10.1002/fld

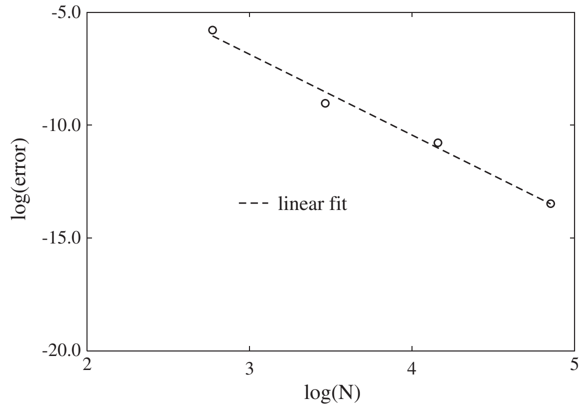

Figure A.1. Order of accuracy test of the central scheme using errors in Taylor–Green vortex flow simulations performed with different resolutions.

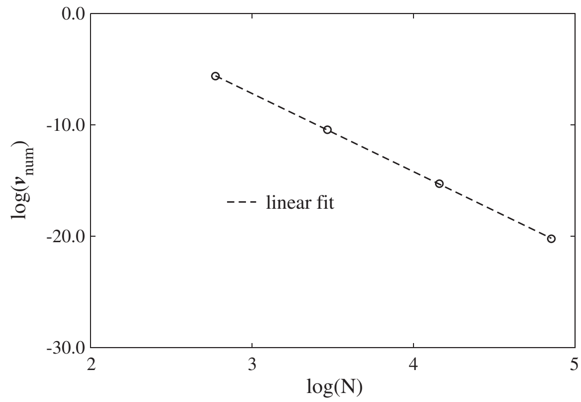

Figure A.2. Dependence of the central scheme's numerical viscosity on grid resolution.

Many of the high-resolution finite volume solvers used for turbulence computations are based on dimensional splitting. One-dimensional higher-order interpolations are used to construct fluxes on cell faces using cell-centered quantities. This is performed because quadrature corrections required to ensure genuinely multidimensional higher-order accurate flux computation are very expensive [46]. As noted by Pirozzoli [6], this practice really results in second-order accuracy. Less than fourth-order accuracy here may also have resulted from dimensional splitting. Ducros and coworkers [68] have investigated the need for quadratures and observed that the errors resulting from dimensional splitting are usually negligible. Claims of higher-order accuracy are often made without using quadrature corrections in case of compact schemes used for turbulence computations.

The simulations are also conducted at various resolutions by setting viscosity to zero. In the inviscid limit, the solution should remain stationary. However, the code predicts very slow decay. Using the preceding formulae, the effective numerical viscosity is computed at each resolution. The effective numerical viscosity is plotted against resolution once again on a logarithmic scale in Figure A.2. A linear fit to this plot has a slope of -7.02, indicating that the dissipative error of the scheme is of the order 7 which is well below 4, the overall order of the scheme.

APPENDIX B: EFFECTS OF NUMERICAL PARAMETERS ASSOCIATED WITH THE SWITCHING FUNCTION

The effect of changing the numerical constant 2.5 in Equation (5) to 1.0 is shown in Figure B.1. This constant relates the weight of the SLAU2 contribution (numerical dissipation) to the amplitude

DOI: 10.1002/fld

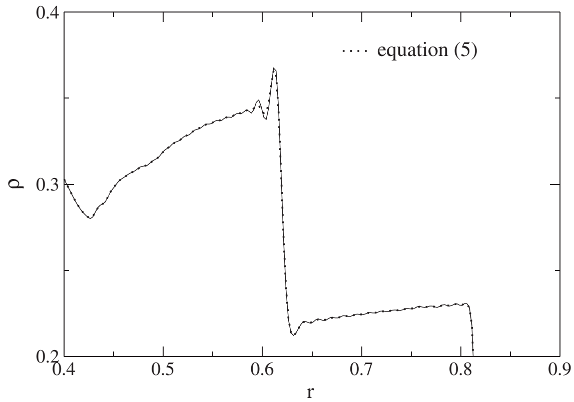

Figure B.1. Effect of changing the numerical constant associated with the unphysical sensor on the solution of the circular blast wave problem. The solid line corresponds to the solution generated using a value of 1.0 instead of 2.5 in Equation (5).

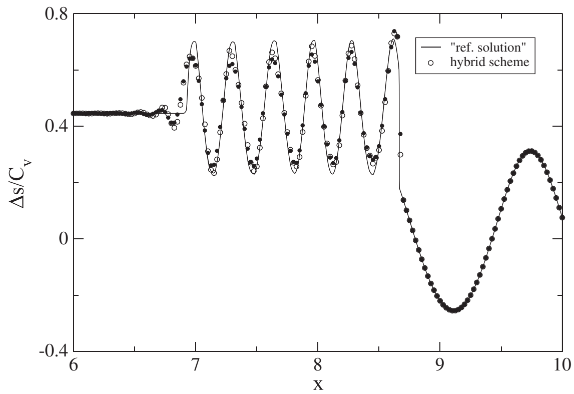

Figure B.2. Effect of changing the constant associated with the discontinuity sensor on the solution of the Shu–Osher problem. The closed symbols correspond to the solution generated by replacing the numerical constant 14 with 8 in Equation (5).

of the unphysical oscillation as detected by the sensor. A higher value of this constant increases the weight of the SLAU2 contribution to the overall flux if unphysical oscillations are detected. With lower values, obviously, the solution is a bit more oscillatory behind the contact line. Increasing the value further (above 2.5) has no noticeable effect. The post-contact line kink in density would still remain. This kink can be reduced if the other constant (i.e., 14) in Equation (5) is adjusted. This constant controls how gradually the central and SLAU2 fluxes are blended. By reducing this constant, the kink will be reduced, but at the expense of extra numerical dissipation. This problem has no physical oscillations; the flow is very smooth away from the shock and the contact line. So, this is not a good choice to demonstrate the problem with additional numerical dissipation.

The dissipative effect of a more gradual switching between the two schemes based on the discontinuity sensor is illustrated in Figure B.2. The entropy fluctuations that are most sensitive to numerical dissipation are damped out if the smoother blending function is used. This problem is chosen for demonstrating this instead of others involving vorticity fluctuations because the damping of vorticity and kinetic energy of SLAU2 is quite low compared with other flux split schemes. The vorticity fields are less affected if switching is made more gradual. The same cannot be said about density fluctuations.

REFERENCES

1. Mittal R, Moin P. Suitability of upwind-biased finite difference schemes for large eddy simulation of turbulent flows. *AIAA Journal* 1997; **35**(8):1415–1417.
2. Morinishi Y, Lund TS, Vasilyev OV, Moin P. Fully conservative higher order finite difference schemes for incompressible flow. *Journal of Computational Physics* 1998; **143**:90–124.
3. Jameson A. The construction of discretely conservative finite volume schemes that also globally conserve energy or entropy. *SIAM Journal of Scientific Computing* 2008; **34**:152–187.
4. Kok JC. A high-order low-dispersion symmetry-preserving finite volume method for compressible flow on curvilinear grids. *Journal of Computational Physics* 2009; **228**:6811–6832.
5. Lele SK. Compact finite difference schemes with spectral-like resolution. *Journal of Computational Physics* 1992; **103**:16–42.
6. Pirozzoli S. Numerical methods for high-speed flows. *Annual Review of Fluid Mechanics* 2011; **43**:163–194.
7. Cook AW, Cabot WH. A high wavenumber viscosity of high-resolution numerical methods. *Journal of Computational Physics* 2004; **195**:594–601.
8. Cook AW, Cabot WH. Hyperviscosity for shock–turbulence interactions. *Journal of Computational Physics* 2005; **203**:379–385.
9. Fiorina B, Lele SK. An artificial nonlinear diffusivity method for shock-capturing in supersonic reacting flows. *Technical Report 57-70*, Annual Research Briefs, Center for Turbulence Research, Stanford University, 2005.
10. Kawai S, Lele SK. Localized artificial diffusivity scheme for discontinuity capturing on curvilinear meshes. *Journal of Computational Physics* 2008; **227**:9498–9526.
11. Johnsen E, Larsson J, Bhagatwala AV, Cabot WH, Moin P, Olson BJ, Rawat PS, Shankar SK, Sjogreen B, Yee HC, Zhong X, Lele SK. Assessment of high resolution methods for numerical simulations of compressible turbulence. *Journal of Computational Physics* 2010; **229**:1213–1237.
12. Fu D, Ma Y. A high order accurate difference scheme for complex flow fields. *Journal of Computational Physics* 1997; **134**:1–15.
13. Pruett CD, Zang TA, Chang C-L, Carpenter MH. Direct numerical simulation of high-speed boundary layer flows-part I: algorithmic considerations and validation. *Theoretical and Computational Fluid Dynamics* 1995; **7**(1): 49–76.
14. Lo SC, Blaisdell GA, Lyrintzis AS. Higher-order shock capturing schemes for turbulence calculations. In *AIAA paper 2007-827*, 2007.
15. Zhang S, Shu C. A new smoothness indicator for the WENO schemes and its effect on the convergence to steady state solutions. *SIAM Journal of Scientific Computing* 2007; **31**:273–305.
16. Zhang S, Jiang S, Shu C. Improvement of convergence to steady state solutions of Euler equations with the WENO schemes. *SIAM Journal of Scientific Computing* 2011; **47**:216–238.
17. Hill DJ, Pullin DI. Hybrid tuned center-difference WENO method for large eddy simulations in the presence of strong shocks. *Journal of Computational Physics* 2004; **194**:435–450.
18. Adams NA, Shariff K. A high-resolution hybrid compact-ENO scheme for shock–turbulence interaction problems. *Journal of Computational Physics* 1996; **127**:27–51.
19. Pirozzoli S. Conservative hybrid compact–WENO schemes for shock–turbulence interaction. *Journal of Computational Physics* 2002; **178**:81–117.
20. Subbareddy PK, Candler GV. A fully discrete, kinetic energy consistent finite-volume scheme for compressible flows. *Journal of Computational Physics* 2009; **228**:1347–1364.
21. Reiss J, Sesterhenn J. *Conservative, Skew-symmetric Discretization of the Compressible Navier–Stokes Equations*, Notes on Numerical Fluid Mechanics and Multidisciplinary Design, vol. 121. Springer: Berlin Heidelberg, 2013.
22. Stolz S, Adams NA. An approximate deconvolution model for large eddy simulations of compressible flows and its application to shock–turbulent-boundary-layers interaction. *Physics of Fluids* 2001; **13**:2985–3001.
23. Adams NA, Stolz S. A subgrid scale deconvolution approach for shock capturing. *Journal of Computational Physics* 2002; **178**:391–426.
24. von Kaenel, Kleiser L, Adams NA, Vos JB. Large-eddy simulation of shock-turbulence interaction. *AIAA Journal* 2004; **42**(12):2516–2528.
25. Grilli M, Schmid PJ, Hickel S, Adams NA. Analysis of unsteady behavior in shockwave turbulent boundary layer interaction. *Seventh European Symposium on Aerothermodynamics*, Brugge, Belgium, 2011.
26. Kawai S, Shankar SK, Lele SK. Assessment of localized artificial diffusivity scheme for large-eddy simulation of compressible turbulent flows. *Journal of Computational Physics* 2010; **229**:1739–1762.
27. Mani A, Larsson J, Moin P. Suitability of artificial bulk viscosity for large-eddy simulation of turbulent flows with shocks. *Journal of Computational Physics* 2009; **228**:7368–7374.
28. Bhagatwala A, Lele SK. A modified artificial viscosity approach for compressible turbulence simulations. *Journal of Computational Physics* 2009; **228**:4965–4969.
29. Yee HC, Sandham ND, Djomehri MJ. Low-dissipative high-order shock-capturing methods using characteristic-based filters. *Journal of Computational Physics* 1999; **150**:199–238.
30. Guo-Hua T, Xiang-Jiang Y. A characteristic-based shock-capturing scheme for hyperbolic equations. *Journal of Computational Physics* 2007; **225**:2083–2097.
31. Shima E, Kitamura K. On new simple low-dissipation scheme of AUSM-family for all speeds. In *AIAA paper 2009-136*, 2009.

DOI: 10.1002/fld

32. Kitamura K, Shima E. Improvements of simple low-dissipation AUSM against shock instabilities in consideration of interfacial speed of sound. *ECCOMAS CFD*, Lisbon, Portugal, 2010.
33. Shima E, Kitamura K. Parameter-free simple low-dissipation AUSM-family scheme for all speeds. *AIAA Journal* 2011; **49**(8):1693–1709.
34. Chakravarthy VK, Chakraborty D. Modified slau2 scheme with enhanced shock stability. *Computers and Fluids* 2014; **100**:176–184.
35. Genin F. Study of compressible turbulent flows in supersonic environment by large eddy simulation. *Ph.D. Thesis*, Georgia Institute of Technology, Atlanta, GA, USA, 2009.
36. Rhie CM, Chow WL. A numerical study of the turbulent flow past an isolated airfoil with trailing edge separation. *AIAA Journal* 1983; **21**(11):1525–1532.
37. Gottlieb D, Turkel E. Dissipative two-four methods for time-dependent problems. *Mathematics of Computation* 1976; **30**:703–723.
38. Nelson C C. Simulations of spatially evolving compressible turbulence using a local dynamic subgrid model. *Ph.D. Thesis*, Georgia Institute of Technology, Atlanta, GA, USA, 1997.
39. Ghia V, Ghia KN, Shin CT. High-resolutions for incompressible flow using the Navier–Stokes equations and a multi-grid method. *Journal of Computational Physics* 1982; **48**:387–411.
40. Ferziger JH, Peric M. *Computational Methods for Fluid Dynamics* (3rd edn). Springer-Verlag: Berlin, Germany, 2002.
41. Harten A. The artificial compression method for computation of shocks and contact discontinuities: III. Self-adjusting hybrid schemes. *Mathematics of Computation* 1978; **32**(142):363–389.
42. Swanson RC, Turkel E. On central-difference and upwind schemes. *Journal of Computational Physics* 1992; **101**:292–303.
43. Ducros F, Ferrand V, Nicoud F, Weber C, Darracq D, Gacherieu C, Poinsot T. Large eddy simulation of the shock turbulence interaction. *Journal of Computational Physics* 1999; **152**:517–549.
44. Visbal MR, Gaitonde DV. Shock capturing using compact-differencing-based methods. In *AIAA paper 2005-1265*, 2005.
45. Larsson J, Lele SK. Direct numerical simulation of canonical shock/turbulence interaction. *Physics of Fluids* 2009; **21**:379–385.
46. Shu C. Essentially non-oscillatory and weighted non-oscillatory schemes for hyperbolic conservation laws. *Technical Report 97–65*, NASA, 1997.
47. Toro EF, Spruce M, Speares W. Restoration of the contact surface in the HLL-Riemann solver. *Shock Waves* 1994; **4**:25–34.
48. Einfeldt B, Munz CD, Roe PL, Sjoreen B. On Godunov-type methods near low densities. *Journal of Computational Physics* 1991; **92**:273–295.
49. Rizzetta DP, Visbal MR, Gaitonde DV. Large-eddy simulation of supersonic compression-ramp flow by high-order method. *AIAA Journal* 2001; **39**(12):2283–2292.
50. Genin F, Menon S. Studies of shock/turbulent shear layer interaction using large-eddy simulation. *Computers and Fluids* 2010; **39**:800–819.
51. Liska R, Wendroff B. Comparison of several difference schemes on 1D and 2D test problems for the Euler equations. *SIAM Journal of Scientific Computing* 2003; **25**:995–1017.
52. Shu CW, Osher S. Efficient implementation of essentially non-oscillatory shock-capturing schemes II. *Journal of Computational Physics* 1989; **83**:32–78.
53. Jiang G, Shu C. Efficient implementation of weighted ENO schemes. *Journal of Computational Physics* 1996; **126**:202–228.
54. Zang TA, Hussaini MY, Bushnell DM. Numerical computations of turbulence amplification in shock-wave interactions. *AIAA Journal* 1984; **22**(1):13–21.
55. Toro EF. *Riemann Solvers and Numerical Methods for Fluid Dynamic* (3rd edn). Springer-Verlag: Berlin, Germany, 2009.
56. Levy D, Puppo G, Russo G. A fourth order central WENO scheme for multidimensional hyperbolic systems of conservation laws. *SIAM Journal of Scientific Computing* 2002; **24**:480–506.
57. Sod GA. A survey of several finite difference methods for systems of nonlinear hyperbolic conservation laws. *Journal of Computational Physics* 1978; **27**:1–31.
58. Quirk J. A contribution to the great Riemann solver debate. *International Journal for Numerical Methods in Fluids* 1994; **18**:555–574.
59. Park JS, Kim C. Multi-dimensional limiting strategy for arbitrary higher-order discontinuous Galerkin methods in inviscid and viscous flows. *Seventh international conference on computational fluid dynamics*, Hawaii, USA, 2012.
60. Bogey C, de Cacqueray N, Bailly C. A shock-capturing methodology based on adaptative spatial filtering for high-order non-linear computations. *Journal of Computational Physics* 2009; **228**:1447–1465.
61. Shu C. High order finite difference and finite volume WENO schemes and discontinuous Galerkin methods for CFD. *Technical Report 2001-11*, ICASE (NASA), 2001.
62. Emery AE. An evaluation of several differencing methods for inviscid fluid flow problems. *Journal of Computational Physics* 1968; **2**:306–331.
63. Woodward PR, Colella P. The numerical simulation of two-dimensional fluid flow with strong shocks. *Journal of Computational Physics* 1984; **54**:115–173. Review article.

64. Billet G, Louedin O. Adaptive limiters for improving the accuracy of the MUSCL approach for unsteady flows. *Journal of Computational Physics* 2001; **170**:161–183.
65. Ghosh D. Compact-reconstruction weighted essentially non-oscillatory schemes for hyperbolic conservation laws. *Ph.D. Thesis*, University of Maryland, College Park, MD, USA, 2012.
66. Hannappel R, Hauser T, Friedrich R. A comparison of ENO and TVD schemes for the computations of shock–turbulence interactions. *Journal of Computational Physics* 1995; **121**:176–184.
67. Sandham ND, Reynolds WC. A numerical investigation of the compressible mixing layer. *Technical Report TF-45*, Stanford University, 1989.
68. Ducros F, Laporte F, Souleres T, Guinot V, Moinat P, Caruelle B. High-order fluxes for conservative skew-symmetric-like schemes in structures meshes: application to compressible flows. *Journal of Computational Physics* 2000; **161**:114–139.